Original Article

Institution of MECHANICAL ENGINEERS

Journal of AUTOMOBILE ENGINEERING

Proc IMechE Part D:
J Automobile Engineering
1–19

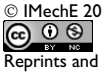
Reprints and permissions:
sagepub.co.uk/journalsPermissions.nav
DOI: 10.1177/0954407017707099
journals.sagepub.com/home/pid
SAGE

Developing a model for analysis of the cooling loads of a hybrid electric vehicle by using co-simulations of verified submodels

Sina Shojaei[1], Andrew McGordon[1], Simon Robinson[2], James Marco[1] and Paul Jennings[1]

Abstract

The requirement for including the air-conditioning and the battery-cooling loads within the energy efficiency analyses of a hybrid electric vehicle is widely recognized and has promoted system-level simulations and integrated modelling, escalating the challenge of balancing the accuracy and the speed of simulations. In this paper, a hybrid electric vehicle model is created through co-simulation of the passenger cabin, the air conditioning, the battery cooling, and the powertrai. Calibration and verification of the submodels help determine their accuracy in representing the target vehicle and achieve a balance between the model fidelity and the simulation speed. The result is a model which has a higher accuracy and a higher speed than those of similar models developed previously and which provides a reliable tool for a thorough investigation of the cooling loads for different ambient conditions and different duty cycles.

Keywords

Vehicle simulations, system-level simulations, co-simulations, hybrid electric vehicle model, energy efficiency of a hybrid electric vehicle, cooling load

Date received: 1 July 2016; accepted: 10 March 2017

Introduction

The energy efficiencie of electric vehicles (EVs) and hybrid electric vehicle (HEVs) are arguably the most critical contributor to their acceptability in today's market. As a result, a significant amount of the research on EVs and HEVs has been motivated by the prospects of a higher energy efficiency. Simulation-based optimisation and model-based optimisation have been key parts of the research, leading to the creation of various simulation tools, such as PSAT,[1] Autonomie,[2] ADVISOR[3] and WARPSTAR.[4] The majority of these tools are based on MATLAB/Simulink and are traditionally centred on the low-fidelity models of the powertrain subsystem, and crude representations of the energy storage, the power electronics and the auxiliary subsystems. Nonetheless, they fit the purpose and have been widely used in driving-cycle calculations, component sizing and energy management optimisation. The need for considering real-world conditions in the calculations has encouraged system-level simulations of EVs and HEVs, by integration of higher-fidelity models of mechanical,[5,6] electrical[7,8] and thermal[9] components or subsystems of the vehicle. Developing high-accuracy models is far more practical in specialised tools than it is in MATLAB/Simulink. Therefore, co-simulation methods are becoming increasingly popular in system-level simulations.[10–12] The compromise between higher fidelity but slower models and lower fidelity but faster models still remains and should be addressed according to the specific application of the model and verification against the experimental data.

Of the auxiliary subsystems on HEVs, the electric air conditioning is the most energy demanding and can have a significant impact on the energy efficiency and the performance of the vehicle.[13–16] The largest load on the electric air conditioning is the thermal load of the

[1]WMG, University of Warwick, UK
[2]Jaguar Land Rover, UK

Corresponding author:
Sina Shojaei, WMG, University of Warwick, Coventry CV4 7AL, UK.
Email: s.shojaei@warwick.ac.uk

passenger cabin,[17] but the refrigeration circuit also provides cooling power to the traction battery[18] and this further increases the power demand of the electric air conditioning. As vehicle batteries become more powerful, their cooling load becomes more comparable with that of the cabin.[18–20] The impact of the cooling load of the cabin and the battery on the energy efficiency can be mitigated in various ways,[21–23] but the first step is to quantify the loads and their impact accurately, either by vehicle tests or, much more practically, by a vehicle-level model. This model should represent both the total the instantaneous cooling loads with sufficient accuracy and still fit the requirement of drive cycle simulations, i.e. flexibility and high speed. Determining the appropriate model fidelity for this purpose has been studied by various researchers.[24–28] The present work is focused on developing a representative model of a chosen vehicle that can support calculation of hot ambient cooling loads within drive cycle energy efficiency simulations. Such applications allow little compromise on the simulation speed owing to their time length. However, based on practical considerations, making use of existing tool and co-simulation techniques is preferable. The approach chosen here is to model the electric air-conditioning subsystem of the target vehicle using the AirConditioning Library of Dymola.[29–31] Models of the passenger cabin and the battery-cooling subsystems are also required. These are developed using the open-source Modelica fluid library and are integrated with the electric air-conditioning subsystem model (submodel). The powertrain of the vehicle, is modelled in WARPSTAR, which is based in MATLAB/Simulink. To ensure that the model is representative of the target vehicle, rigorous calibration and experimental verification are carried out at the subsystem level. The vehicle model is then constructed from verified submodels which are co-simulated in Simulink with the help of the Functional Mock-up Interface (FMI) standard.[32] Subsystem-level and vehicle-level verifications prove that the model is sufficiently accurate and the simulation speed is sufficiently fast; therefore, the vehicle model is suitable for the intended applications. In fact, as discussed, the achieved levels of accuracy and simulation speed are better than or at least comparable with similar models proposed previously in literature.

The main contribution of this paper is that it introduces a new tool for system-level simulations of hybrid vehicles, while outlining the achieved level of accuracy and the required modelling effort across a range of subsystems. The paper is organised in the following order. The next section introduces the target vehicle and describes the details of the relevant subsystems. The sunbsequent sections explain the submodels and the corresponding verification approach. Then, the model integration and co-simulation process as well as verification of the vehicle-level energy efficiency calculations are outlined. Finally, the scope of the follow-on work and a summary of the current research results are presented.

The target vehicle

A simplified illustration of the subsystems of the target vehicle is given in Figure 1. This vehicle has an all-wheel-drive parallel hybrid electric powertrain in which a 140 kW diesel engine is coupled to the driveline via a clutch, and a 35 kW electric machine is integrated within the transmission pre-gearbox. The battery pack has 72 cylindrical cells, each with 6.7 A h capacity, which are organised in six modules. The electrical architecture of the pack is 72S1P (72 cells in series).

Other subsystems of the vehicle which are of interest are the battery cooling, the electric air conditioning and the passenger cabin. As seen in Figure 1, the battery-cooling circuit includes a pump, an expansion tank and a cooling pipe and is integrated into the refrigeration circuit of the electric air-conditioning subsystem using a refrigerant–coolant heat exchanger (a chiller). The electric air-conditioning subsystem is composed of a refrigeration circuit and air-handling units. The refrigeration circuit, seen in Figure 1, is composed of a 33 cm^3 constant-displacement variable-speed electric compressor, two air–refrigerant heat exchangers (an evaporator core and an integrated condenser–subcooler core), an internal refrigerant–refrigerant heat exchanger (IHX), as well as the chiller. The dimensions and the power ratings of the heat exchanger cores are given in Table 1. Two thermostatic expansion valves (TXVs) with integrated shut-off regulate the superheat and the allocation of cooling power to the evaporator and the chiller.

The passenger cabin in this vehicle (not shown in Figure 1) is approximately 2900 mm long and 1700 mm wide, with a shell made of 4.2 m^2 of glass (i.e. the windscreen, side windows, rear window, etc.) and 5.2 m^2 of wall segments (i.e. doors, side posts and the roof). A model is developed for each of the above vehicle subsystems, and the modelling and verification processes are detailed in the following sections.

The cabin subsystem

Vehicle cabin models are often developed and used for a variety of purposes, such as calculating the thermal loads,[33–35] designing the ventilation systems[36,37] and understanding the localised thermal conditions experienced by passengers;[38–41] therefore, such models have various degrees of fidelity and complexity. When the primary aim is to calculate the overall thermal conditions of the cabin, lengthy simulations can be avoided by using lumped-parameter models which neglect the spatial distribution of temperature and the irregularity of materials within the cabin. The cabin model developed in the current work is based on this approach.

Modelling the cabin

In contrast with the majority of the lumped-parameter models proposed previously which use the orientation

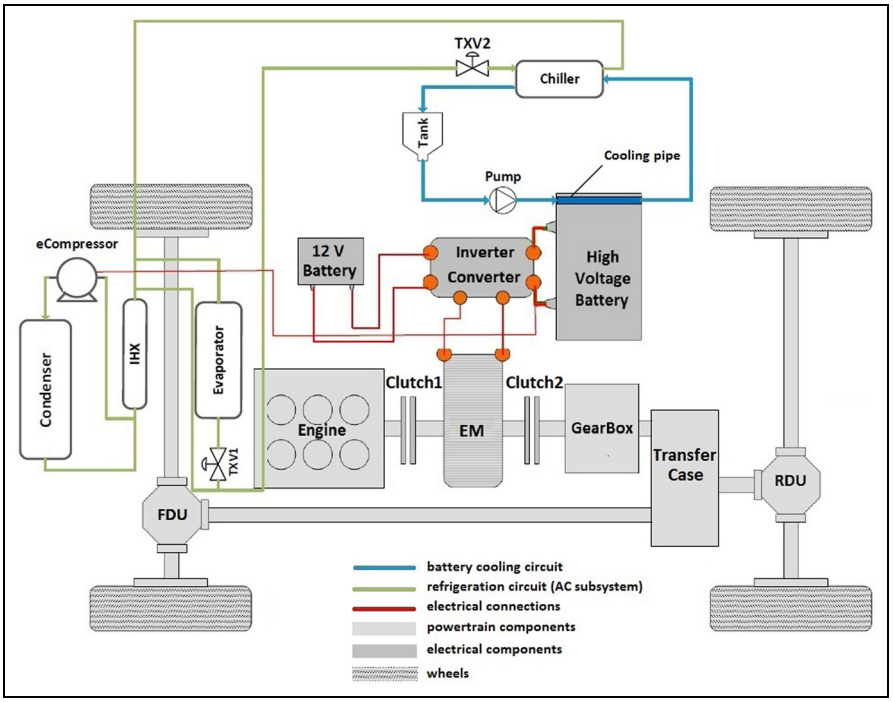

Figure 1. Vehicle subsystems.
TXV2: thermostatic expansion valve 2; eCompressor: electric compressor; IHX: internal refrigerant–refrigerant heat exchanger; TXV1: thermostatic expansion valve 1; EM: electric machine; FDU: front drive unit; RDU: rear drive unit.

Table 1. Heat exchanger specifications.

Component	Dimensions (mm × mm × mm)	Rated capacity (kW)	Type
Condenser	570 × 593 × 16	19	Parallel flow
Evaporator	235 × 293 × 50	9	Cross flow
Chiller	87 × 43 × 62	3	—

of the shell to calculate the solar heat gain,[35,42,43] we assume the significantly simpler geometry in Figure 2, in which the glass and walls forming the cabin shell are modelled as lumped horizontal blocks with areas equal to the total area of glass or wall segments in the cabin shell, and their material properties and temperatures are averaged around the cabin.

The cabin air is represented by a lumped air volume with ideal mixing as proposed previously[35,41,42,44] and thermal interactions with the shell and the interiors. In addition to the mass transfer due to ventilation and leakage, the major heat flows that affect the thermal conditions of the vehicle cabin are the solar irradiance, the convection between the shell and the ambient air, the conduction through the shell, the convection between the cabin air and the shell, the convection between the cabin air and the interior, the radiation from the glass and the interior, as well as the heat rejection from passengers. Possible thermal interactions with the engine compartment were ignored. It is also assumed that the heat transfer through the floor is limited to that from the battery.

The thermal interactions of the cabin are modelled by using first principles; however, to compensate for the simplifications in the cabin geometry, a number of shape factors are considered which are identified by calibration with the test results. For example, the solar irradiance absorbed by the cabin glass is modelled as

$$\dot{Q}^{irr}_{g,\,abs} = k1^{irr}_{g}\alpha_g \ \mathrm{SI}\ A_g \tag{1}$$

where $k1^{irr}_{g}$is the shape factor included to account for the variability in the inclination, the curvature and the coatings of the different glass surfaces. A similar model is considered for the irradiance absorbed by the walls. The solar irradiance transmitted through the glass is consequently calculated as

$$\dot{Q}^{irr}_{g,\,tr} = k1^{irr}_{g}\tau_g \ \mathrm{SI}\ A_g \tag{2}$$

where SI is the solar irradiance. Although a large part of the transmitted component of the solar irradiance is absorbed by the interior, some part of it can continue to exit the cabin environment. Therefore, to approximate the total transmitted irradiance incident that

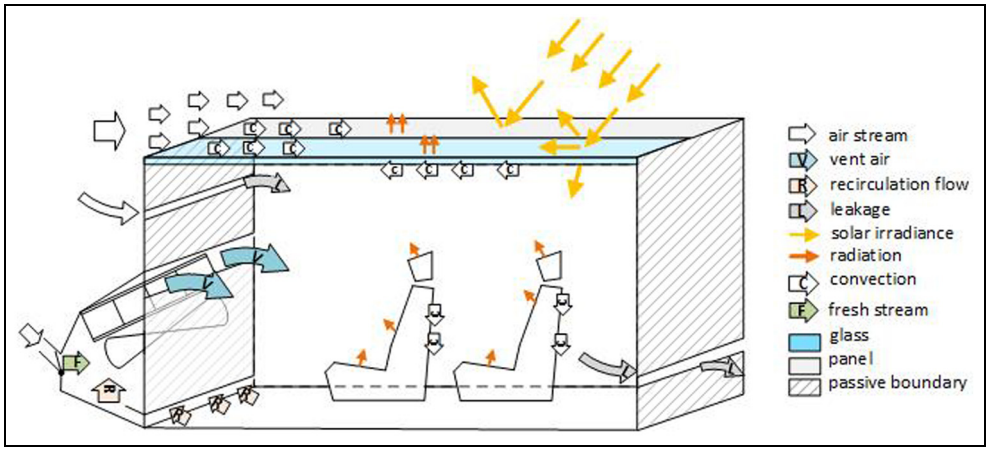

Figure 2. Geometry assumed by the model.

affects the interior of the cabin, equation (2) is modified by a correction factor $k2_{int}^{irr}$ to give

$$\dot{Q}_{int,\,abs}^{irr} = k2_{int}^{irr}\left(k2_{g}^{irr}\tau_g \text{ SI } A_g\right) \quad (3)$$

In modelling the interior of the cabin (seats, dashboard, floor and wall carpets, etc.), two separate heat capacities are used. This is to account for the fact that the upper parts of the interior are more exposed to the solar irradiance and can reach significantly higher temperatures. The total heat capacity and surface area of the interior was then split between the upper interior and the lower interior.

The heat transfer to the air enclosed in the cabin occurs primarily by convection. In modelling the convection between the cabin air and the interior, an average heat transfer coefficient as a function of the interior air flow was used, on the basis of the method proposed by Nielsen et al.[33] and Zhang et al.[36] Once the total heat flow to cabin air is calculated, the net internal energy of the cabin air can be calculated from the first law of thermodynamics on the assumption that air enters and exits the cabin at the same flow rate. The above approach leads to a total of four unknown parameters (the split between the heat capacities of the lower interior and the upper interior, in addition to three shape factors) that should be calibrated to complete the description of the required thermal interactions.

Calibration and verification

To calibrate the cabin model, the data obtained from pull-down tests and hot-soak tests of the target vehicle in a climatic chamber are used. These tests are part of the standard procedure for evaluating mobile air-conditioning systems.[39,45] The aim of the pull-down test is to determine the time and the energy required to cool the cabin in hot climate conditions. Typically, the vehicle is placed in the climatic chamber for 3 h in the conditions given in Table 2. The air-conditioning system is switched on at the maximum power, and the vehicle is driven over a purpose-built driving cycle. With the assumed conditions, a complete pull-down test of the target vehicle from 60 °C to 24 °C takes about 4300 s (approximately 1 h 12 min). The aim of the hot-soak test is to determine the maximum temperature experienced inside the cabin in an extremely hot climate; thus, the vehicle is placed in the climatic chamber until saturation temperatures are reached. The air temperature and the flow rate, as well as the temperatures of the shell and the interior, were measured at various points.

Table 2. Climate chamber conditions for pull-down and hot-soak tests.

Air temperature (°C)	Solar irradiance (W/m^2)	Relative humidity (%)	Windows
43	850	60%	Closed

The pull-down tests and the hot-soak tests were simulated with the ambient conditions, the irradiance, the vehicle speed, the air flow rate and the average vent temperatures as the boundary conditions, and the calibration factors were determined through linear regression.

Using the calibrated model, a new pull-down and hot soak test was simulated to verify the model. The measured and simulated cabin air temperatures are compared in Figure 3. It can be seen that very close correlation was achieved, which verifies the suitability of the model for predicting the cabin air temperature in both the cooling scenario and the warming scenario.

Battery-cooling subsystem

As shown in Figure 4, the thermal model of the battery is represented by a heat capacity with thermal interaction with the coolant within the cooling pipe and the ambient air. This model does not distinguish between individual cell temperatures.

The heat balance equation of the battery in this model is

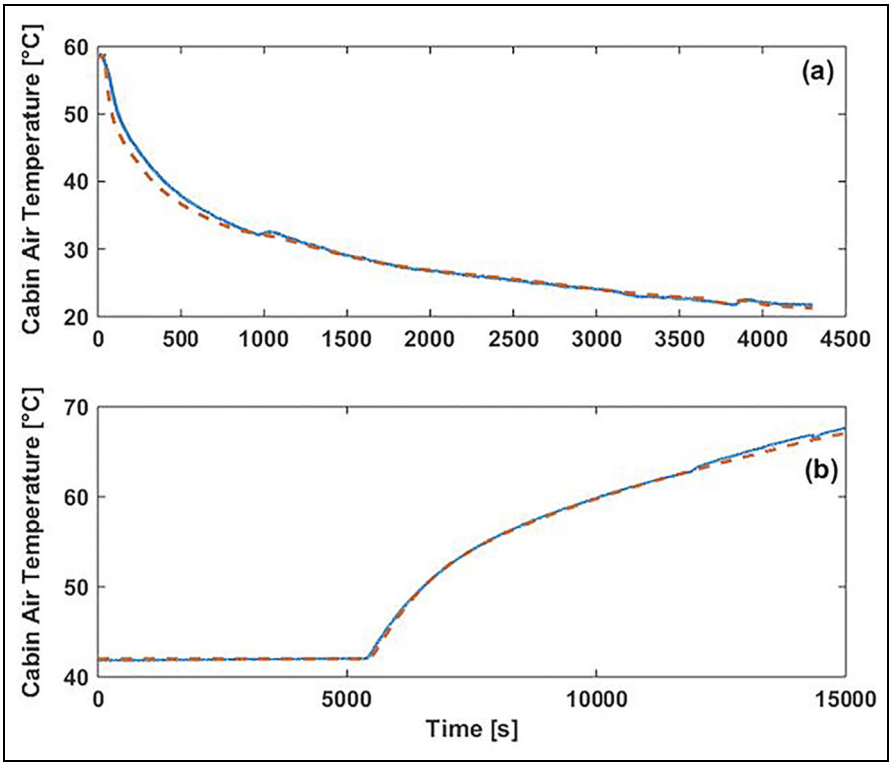

Figure 3. Verification of the cabin model against (a) pull-down tests and (b) hot-soak tests: solid curves, test results: dashed curves, simulation results.

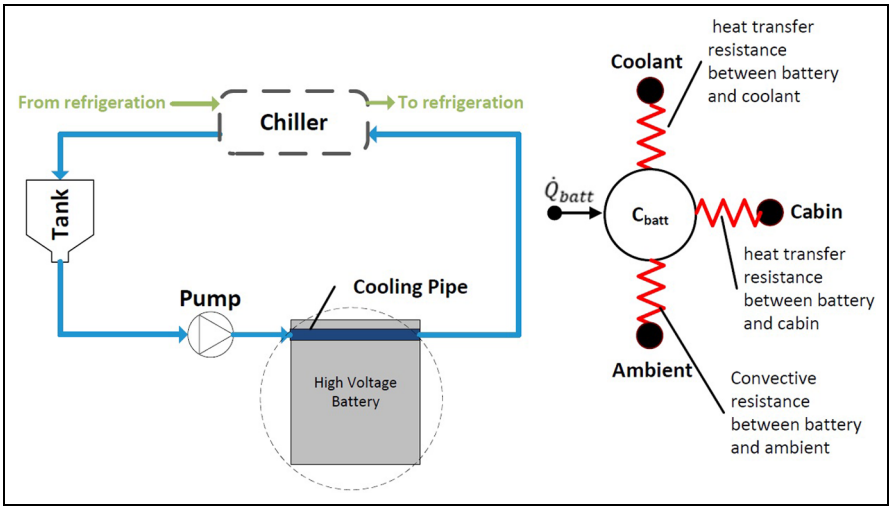

Figure 4. Layout of the battery-cooling circuit.

$$\dot{Q}_{amb} + \dot{Q}_{cabin} + \dot{Q}_{clnt} + \dot{Q}_{gen} - C_{batt}\frac{\mathrm{d}T_{batt}}{\mathrm{d}t} = 0 \quad (4)$$

in which the heat transfer between the battery and its ambient is given by

$$\dot{Q}_{amb} = \frac{T_{amb} - T_{batt}}{R_{amb}} \quad (5)$$

the heat transfer between the battery and the interior of the cabin is given by

$$\dot{Q}_{cabin} = \frac{T_{cabin,\,int} - T_{batt}}{R_{cabin}} \quad (6)$$

and the heat transfer to the coolant is given by

$$\dot{Q}_{clnt} = \frac{\Delta T_{ln}}{R_{clnt}} = \dot{m}_{clnt} c_{clnt} (T_{clnt,\,out} - T_{clnt,\,in}) \quad (7)$$

where ΔT_{ln} is the logarithmic average of the temperature between the battery and the coolant along the

Table 3. Parameters of the battery-cooling subsystem.

Parameter	Value
A_{amb}	0.432 m^2
R_{amb} (0 km/h)	0.9 K/W
R_{amb} (50 km/h)	0.47 K/W
R_{clnt}	0.002 K/W
R_{cabin}	0.06 K/W
c_{clnt} (at 25 °C)	3.65 kJ/kg K

length of the cooling pipe. Heat generation within the battery is associated solely with Joule heating[46] in this model because other mechanisms of heat generation have little significance for traction batteries and were therefore neglected.[47] A list of key parameters of the battery-cooling subsystem is given in Table 3. Verification of the model is carried out in conjunction with the air-conditioning subsystem model in the following section.

Air-conditioning subsystem

The air-handling unit of the air-conditioning subsystems include the ducts, the vents, the evaporator blower, the condenser (radiator) fan and the air heater. These components were briefly modelled as follows. The air ducts are modelled as frictionless pipes and volumes. The evaporator blower was modelled by implementing the blower characteristic curve as a look-up table. The condenser fan was modelled similarly; however, the total condenser air flow was implemented as a function of the vehicle speed. Also, an ideal air heater model is used to allow reheating of the air stream which exits the evaporator. The rest of this section covers the model developed for the refrigeration circuit of the air-conditioning subsystem.

Modelling the refrigeration circuit

The layout of the refrigeration circuit is shown in Figure 5. Various specialised tools[29,30,44,48–50] exist for modelling the refrigeration cycles which facilitate the implementation and solution of the equations that describe the thermodynamics of refrigeration. In the present work, the Dymola AirConditioning Library is used, because, despite the fact that it uses a one-dimensional model, it has been shown to represent the steady-state behaviour and transient behaviour of the electric air conditioning with sufficient accuracy. It is beyond the scope of this paper to discuss the refrigeration circuit models in detail. A full explanation can be found in the work by Shojaei et al.,[22] Eborn[51] and Tummescheit.[52] For completeness, a summary of the key attributes pertinent to the problem under investigation are provided for reference, with emphasis on the heat exchangers because of their higher complexity.

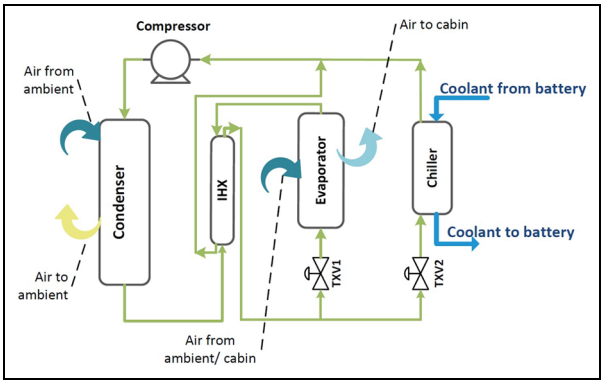

Figure 5. Layout of the refrigeration cycle.
IHX: internal refrigerant–refrigerant heat exchanger; TXV1: thermostatic expansion valve 1; TXV2: thermostatic expansion valve 2.

Heat exchangers. Basic models of typical heat exchangers similar to those used in the refrigeration circuit in Figure 5 are available in the simulation tool. These models are developed based on the (staggered) control volume approach.[52,53] To customise the existing models for specific components of interest, the constitutive equations (the relationships for the pressure drop and the heat transfer) should be defined through parameterisation and calibration of the models. This process is detailed below as it is key to achieving an accurate calculation of the cooling power available to the cabin and the battery.

For the air–refrigerant heat exchanges (condenser and the evaporator in Figure 5), the air-side heat transfer model and the refrigerant-side heat transfer model are implemented in the general forms

$$\dot{Q}_{aw} = \bar{h}_{aw} A_{aw} (T_{air} - T_w) \tag{8}$$

and

$$\dot{Q}_{wr} = \bar{h}_{wr} A_{wr} (T_w - T_r) \tag{9}$$

respectively, where A_{aw} and A_{wr} are the heat transfer areas which can be defined by using the parameterising geometries. In this work, the heat exchanger geometries were accurately defined using a combination of manufacturer drawings and component measurements. $\bar{h}_{aw}$ and $\bar{h}_{wr}$ are functions of the Nusselt number Nu, the fluid properties and the heat exchanger geometry. Once the geometries are known, the Nusselt number is the only unknown but it can be determined using empirical models and calibration. It was assumed here that the heat flux on the air side of the heat exchanger is the limiting factor. Therefore, for the refrigerant-side heat transfer, the Nusselt number is assumed to be consistent with the Dittus–Boelter model[54] and is given by

$$Nu = 0.023\ Re^{4/5}\ Pr^{n} \tag{10}$$

where the exponent $n = 0.3$ for heat absorption (evaporator) and $n = 0.4$ for heat rejection (condenser).

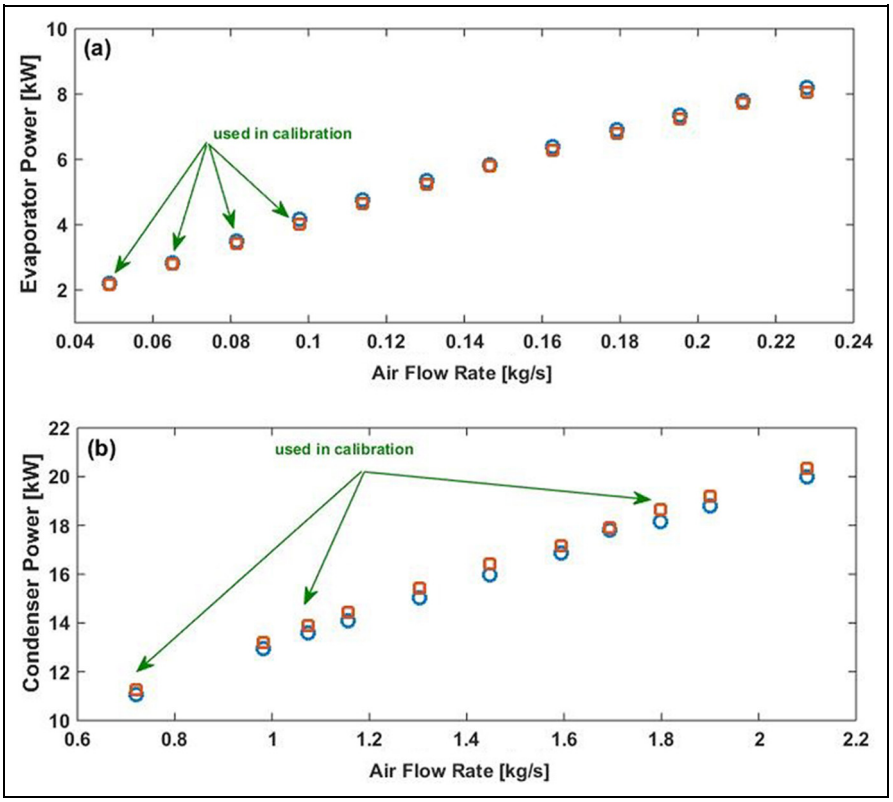

Figure 6. Calibration and verification of heat transfer models in the air–refrigerant heat exchangers showing (a) the evaporator power and (b) the condenser power: open circles, test results; open squares, simulation results.

For the air-side heat transfer, the Nusselt number was implemented in the general form (see equation (7-1) in the book by Incropera[54])

$$Nu = C_1 \, Re^{C_2} \, Pr^n \tag{11}$$

where the coefficients C_1 and C_2 can be calibrated from the experimental data. A set of component characterisation data was available for this purpose, in which the cooling power of the heat exchanger is calculated in steady-state conditions. The characterisation procedure is briefly as follows. The refrigerant enters the heat exchanger at a specified pressure and subcooled conditions and exists at the pressure set on the heat exchanger outlet. A stream of air at a specified temperature and humidity is blown on to the heat exchanger and is cooled or heated as it exits. The mass flow rate of the refrigerant is adjusted to achieve the required superheat for any air flow rate, and the resulting cooling power is measured. Simulating the component models with the boundary conditions of the test, the corresponding Reynolds number and the corresponding Nusselt number can be calculated from the flow conditions and the calculated cooling power. The coefficients C_1 and C_2 in equation (12) were then found by linear regression over a number of the available measurement points and replaced in the models. The models were then verified by comparing the simulations and the test results for the remaining measurement points. As Figure 6 shows, this process resulted in an accuracy of $\pm 5\%$, which is acceptable for the purpose of this model.

The customisation process for the liquid–liquid heat exchangers (the IHX and the battery chiller in Figure 5) is fundamentally similar to that explained above: defining the geometries and calibrating the heat transfer models. For the refrigerant side of the chiller the Dittus–Boelter correlation (equation (11)) is used. For the IHX, since the flow is single phase, empirical correlations for single-phase flows in circular pipes are used.[55] To compensate for the geometric incompatibilities, a correction factor was assumed, leading to

$$\bar{h}_{corrected} = k\bar{h} \tag{12}$$

where $\bar{h}$ is the heat transfer coefficient given by empirical correlations and the correction factor $k = 0.90$ was defined by calibration. The resulting heat flows are plotted against the measured data in Figure 7 and show that close correlations were achieved.

A similar calibration and verification approach was employed to define the pressure loss models of the heat exchangers. In the interest of brevity, this process is not discussed further in this work.

Mass flow devices. The compressor and the valves of the circuit of Figure 5 are modelled by simple algebraic equations, since their dynamics are much faster than the average dynamics of refrigeration.[56] The

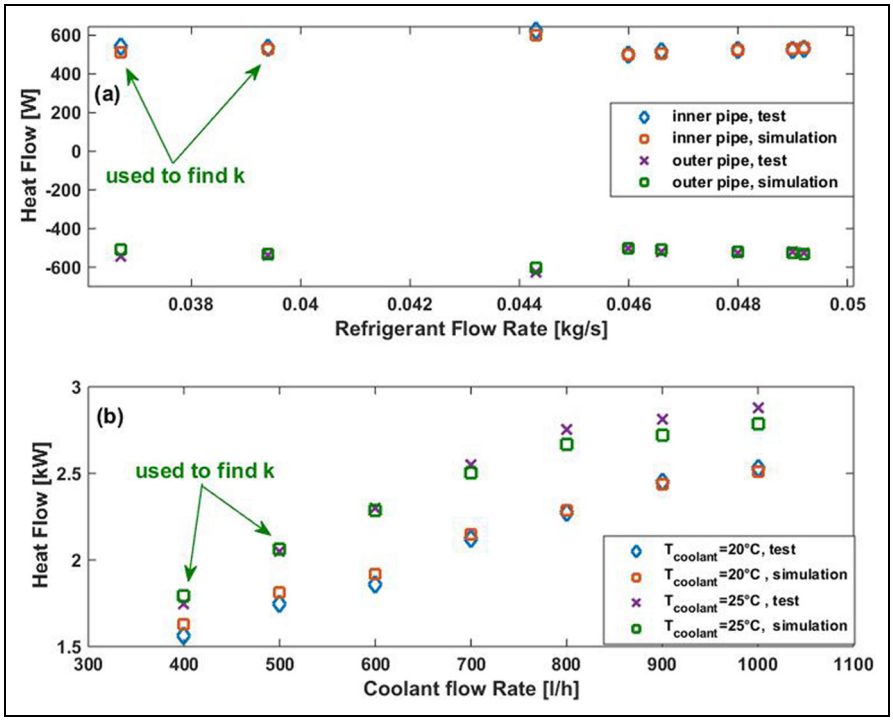

Figure 7. Calibration and verification of the heat transfer models in the internal flow heat exchangers: (a) the IHX; (b) the chiller.

compressor is modelled by describing the ideal mass flow rate of the refrigerant as a function of the rotational speed, the displacement and the volumetric efficiency, on the assumption of adiabatic compression. The isentropic efficiency map of the compressor is then required to correct the enthalpy values. The efficiency maps were extracted from the component data sheets for the purpose of this work. The electrical efficiency of the compressor was assumed to be 85% independent of its voltage. On the other hand, valve models consist of a volume and a simple pressure loss model with a variable flow coefficient. In the TXV models, the flow coefficient is controlled by a proportional–integral (PI) controller which mimics the behaviour of the mechanical components of the valve.

Steady-state verification of the refrigeration circuit

After the full circuit model in Figure 5 was constructed from the above components, verification at the circuit level was desirable. Steady-state characterisation of the vehicle's refrigeration circuit was carried out on a test rig at nine test points, and the data set was used to verify the model. The verification results plotted in Figure 8 imply good correlation. The errors in the simulated chiller temperatures and simulated evaporator temperatures in Figure 8(b) and Figure 8(c) respectively are less than 3 °C. Also the refrigerant pressures on both the high-pressure side and the low-pressure side were predicted with ±1.5 bar error. These results imply an accuracy which is similar to or better than those given by the models of equivalent fidelity proposed by Huang et al.,[24] Kiss et al.[44] and Braun et al.[51] Transient verification of the model is discussed in the following section.

Transient verification of the refrigeration circuit and the battery-cooling circuit

For transient verification of the refrigeration circuit, the vehicle was tested in a climatic chamber at 43 °C. The refrigeration circuit and the battery-cooling circuit were instrumented. Here, as seen in Figure 9, the refrigeration circuit model and the battery-cooling circuit model are integrated. The battery average temperature, the TXV2 flag, the evaporator inlet air temperature and the compressor velocity are used as inputs. The condenser air flow rate is calculated from the vehicle speed, and the evaporator air flow is known from the fan specifications.

Figure 10 shows the on–off flag of the battery chiller TXV (TXV 2) and the compressor speed, which are the control signals and have the highest transients compared with the other inputs to the models.

In Figure 11 the simulated temperatures and the measured temperatures of the average evaporator air-off, the coolant at the battery inlet and the average condenser air-off are compared. As the figure shows, the model represents all the major system dynamics with an absolute error of less than 4 °C. A possible reason behind this inaccuracy is that the presence of lubrication oil in the refrigeration circuit and its potential impact on the heat transfer properties of the refrigerant are neglected.

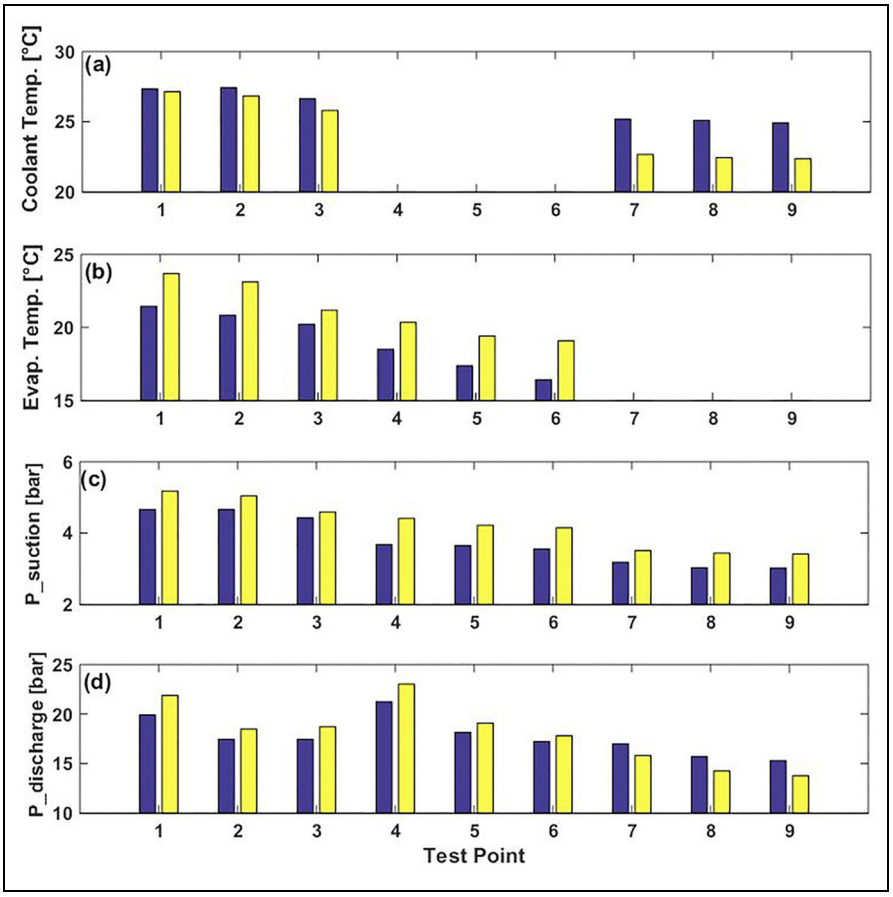

Figure 8. Verification of the refrigeration circuit model against the test rig measurement for (a) the coolant temperature at the chiller outlet, (b) the average evaporator air temperature, (c) the suction pressure and (d) the discharge pressure: black bars, test results: light bars, simulation results. For test points 1 to 3, both the evaporator and the chiller are in the circuit; for test points 4 to 6, only the evaporator is present in the circuit (the chiller is isolated); for test points 7 to 9, only the chiller is present in the circuit (the evaporator is isolated).
Temp.: temperature; Evap.: evaporator.

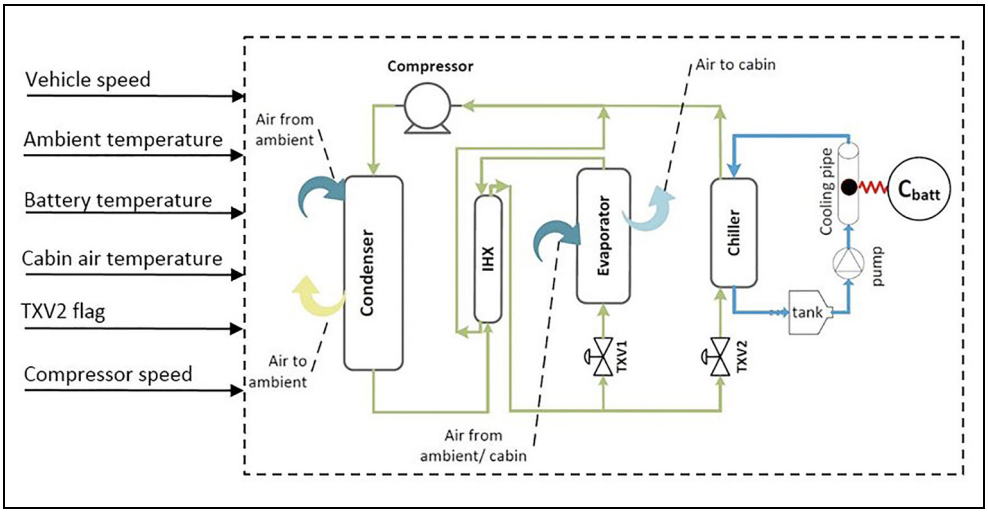

Figure 9. Integrated refrigeration and coolant circuits as assumed for transient verification.
IHX: internal refrigerant–refrigerant heat exchanger; TXV1: thermostatic expansion valve 1; TXV2: thermostatic expansion valve 2.

Figure 12(a) and Figure 12(b) show that the model was able to calculate the refrigerant pressure at the suction port and the discharge port of the compressor, leading to a reasonably accurate calculation of the compressor power (Figure 12(c)). The results achieved here are more accurate than those reported by Nielsen

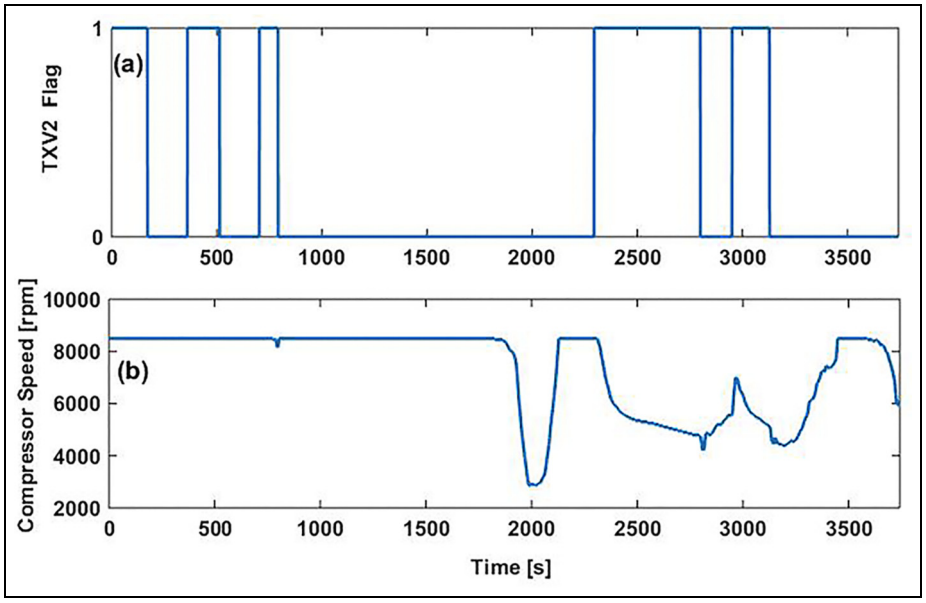

Figure 10. Control signals used as the inputs to the model in the verification process: (a) flag signal of TXV 2; (b) the compressor velocity.
TXV2: thermostatic expansion valve 2; Comp. Vel.: compressor velocity; rpm: r/min.

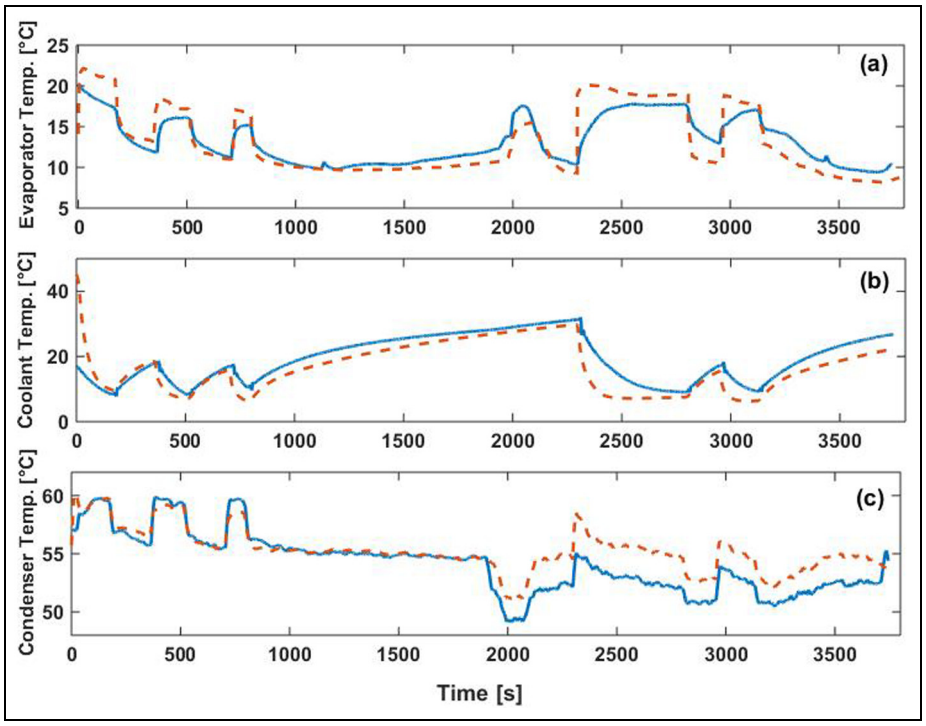

Figure 11. Verification results of the integrated refrigeration and battery-cooling circuit model against the transient vehicle data for (a) the average evaporator (air) temperature, (b) the coolant temperature and (c) the condenser temperature: solid curves, test results; dashed curves, simulation results.
Temp.: temperature.

et al.[33] and Orofino et al.[57] and are comparable with the results reported by Ling et al.;[28] therefore, it can be concluded that the air-conditioning submodel and the battery-cooling submodel are appropriate for the intended application.

The powertrain subsystem

The powertrain model was developed in WARPSTAR on the basis of the longitudinal dynamics of the vehicle with the general form

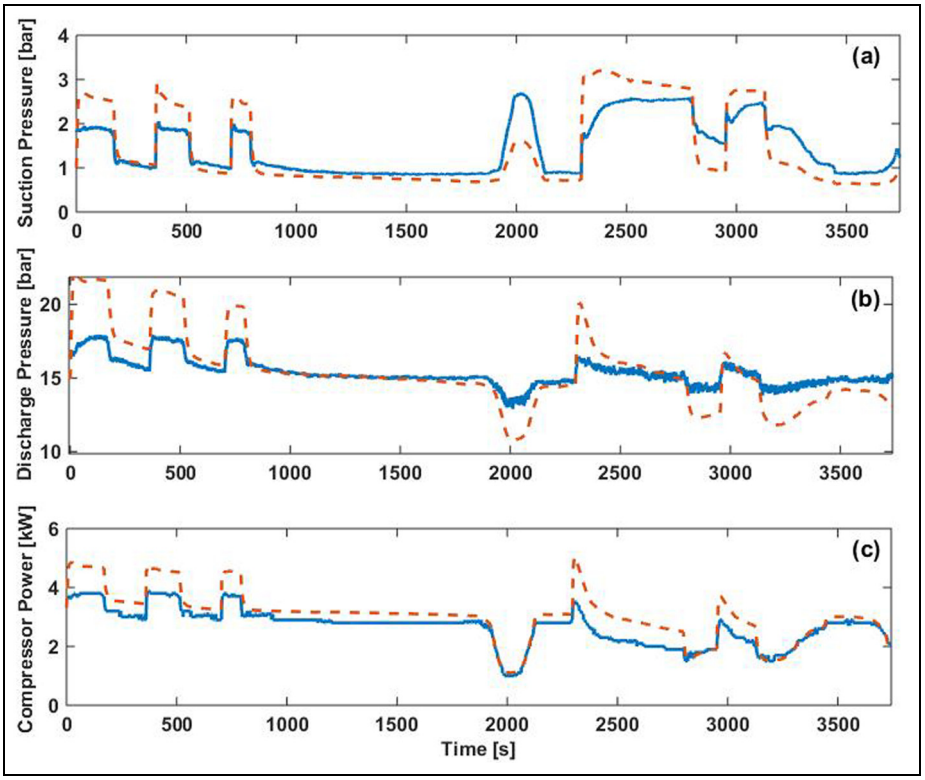

Figure 12. Verification results of the integrated refrigeration and battery-cooling circuit model against the transient vehicle data for (a) the compressor suction pressure, (b) the compressor discharge pressure and (c) the compressor electric power: solid curves, test results; dashed curves, simulation results.

Table 4. Conditions for the powertrain characterisation test.

Condition	Setting	Condition	Setting
Ambient temperature	25 °C	D.c.-to-d.c. converter	Disconnected
Temperature of the battery[a]	30 °C	12 V loads	Free
State of charge of the battery[a]	54.7%	Air-conditioning compressor	Off
Temperature of the engine oil[a]	25 °C	Drive cycle	NEDC
Battery coolant pump	Active		

NEDC: New European Driving Cycle.
[a]Initial values.

$$\frac{\eta\beta}{R}\left[\tau_{eng}\left(\frac{\eta\beta v}{R},\theta\right)+\tau_{em}\left(\frac{\eta\beta v}{R}\right)\right]-F_{RR}-F_A=\left(M+\frac{I_{eq}}{R^2}\right)\frac{dv}{dt} \quad (13)$$

Details of the equations have been given in the relevant documents and literature.[4] Once the model was parameterised for the target vehicle, experimental verification was required. The vehicle was tested on a chassis dynamometer, and its controller area network signals were logged. Details of this test were consistent with the European Union test procedures.[58] Table 4 lists the details most relevant to this work.

The dynamometer test enables verifications at both component level and subsystem level. The intention here is to outline the process and to illustrate the level of accuracy which the component models deliver. Therefore, the discussions are limited to verification of the engine and the complete powertrain model.

Component-level verification

To verify the engine model, it was simulated with logged brake torque and angular velocity signals as the inputs. The simulated and logged fuel consumption values were then compared, as in Figure 13.

The simulated fuel flow rate in the above figure is consistent with the inputs. However, an offset between the simulated fuel flow rate signals and the logged fuel flow rate signals is seen (which is more obvious over cruise periods) and led to 11% underestimation of the total consumed fuel over the driving cycle. This error is due to the low fidelity since only hot engine fuel maps at 90 °C and high-temperature driveline efficiency maps

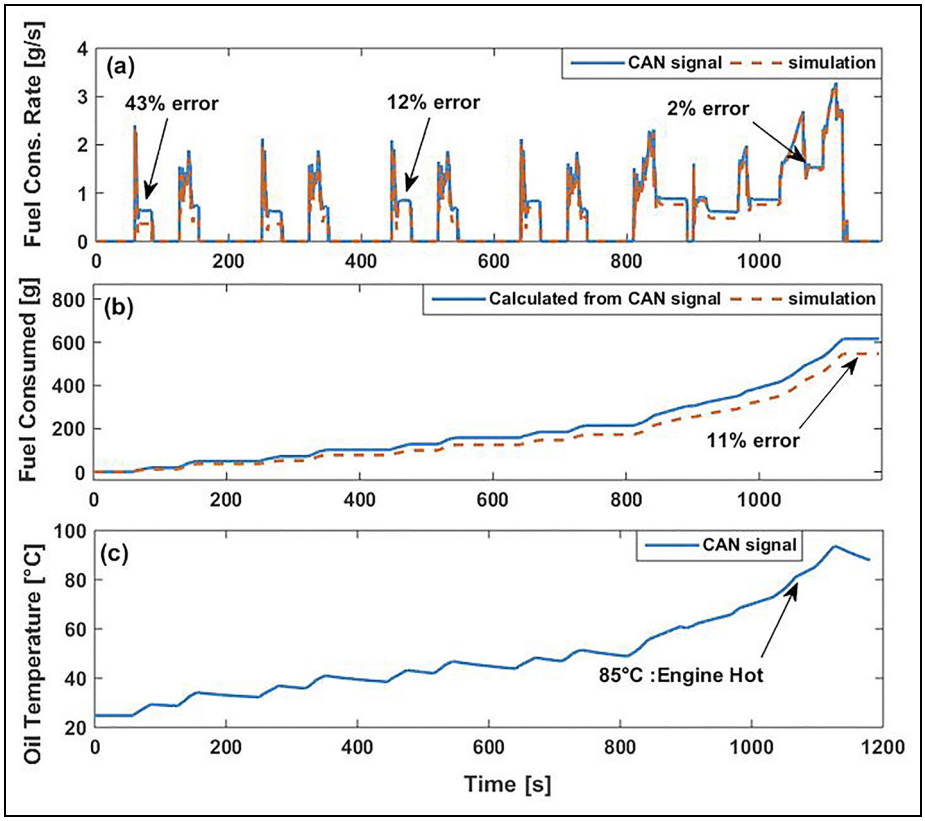

Figure 13. Engine model verification results for (a) the fuel flow rate, (b) the total fuel consumed against the test results and (c) the variations in the oil temperature: solid curves, test results; dashed curves, simulation results.
Cons.: consumption; CAN: controller area network.

were used in the model. According to the test regulations, the vehicle starts cold (from 25 °C); thus, the error is large in the beginning but fades away as the components gradually warm up. The issue can be resolved by modelling the thermal behaviour of the engine and driveline components and interpolating between the hot maps and the cold maps at the cost of increased computation but, since the intended application is simulating hot-climate scenarios, the level of accuracy seen in Figure 13 is considered sufficient.

Subsystem-level verification

Verification of the complete powertrain model can be achieved by simulating it with the logged vehicle speed profile as the input. It is worth mentioning that, since the exact control algorithms of the target vehicle are not used, any comparison between the simulations and the test results at this level are inevitably prone to error but are helpful for understanding the overall performance of the control rules and for identifying areas for improvement. Figure 14 compares the logged and simulated engine velocities and torques and the logged and simulated electric machine velocities and torques, as well as the battery state-of-charge (SoC) signals. This figure shows an acceptable correlation between the engine velocities and the electric machine velocities, which also indicates that the rule-based controller closely reconstructed the major operation modes of the vehicle, i.e. low-speed drive in the EV mode, hybrid drive above 24 km/h, engine stop and regeneration, etc. Although some of the discrepancies seen in the engine torques and the electric machine torques are due to noise, the majority are driven by the error in the SoC. The logged SoC decreases more rapidly than the model estimates, dropping below the lower limit of 50% earlier and shifting the charge event in time, as indicated in Figure 14(d) and Figure 14(e). A closer investigation of the results shows that this error is in fact due to an inaccuracy in the current measurements rather than to a model inaccuracy. Similar observations prove that simulation results were consistent with the assumed model fidelity and control rules, suggesting that the powertrain model is suitable for the intended application.

Model integration

The vehicle model was developed by co-simulations of the above submodels in Simulink. For vehicle energy efficiency simulations, it is common to discretise vehicle driving cycles with discretisation steps as large as 1 s. This helps to improve the simulation speed without compromising the accuracy required for these simulations. Therefore, the powertrain model should be simulated with discrete fixed-step solvers. On the other

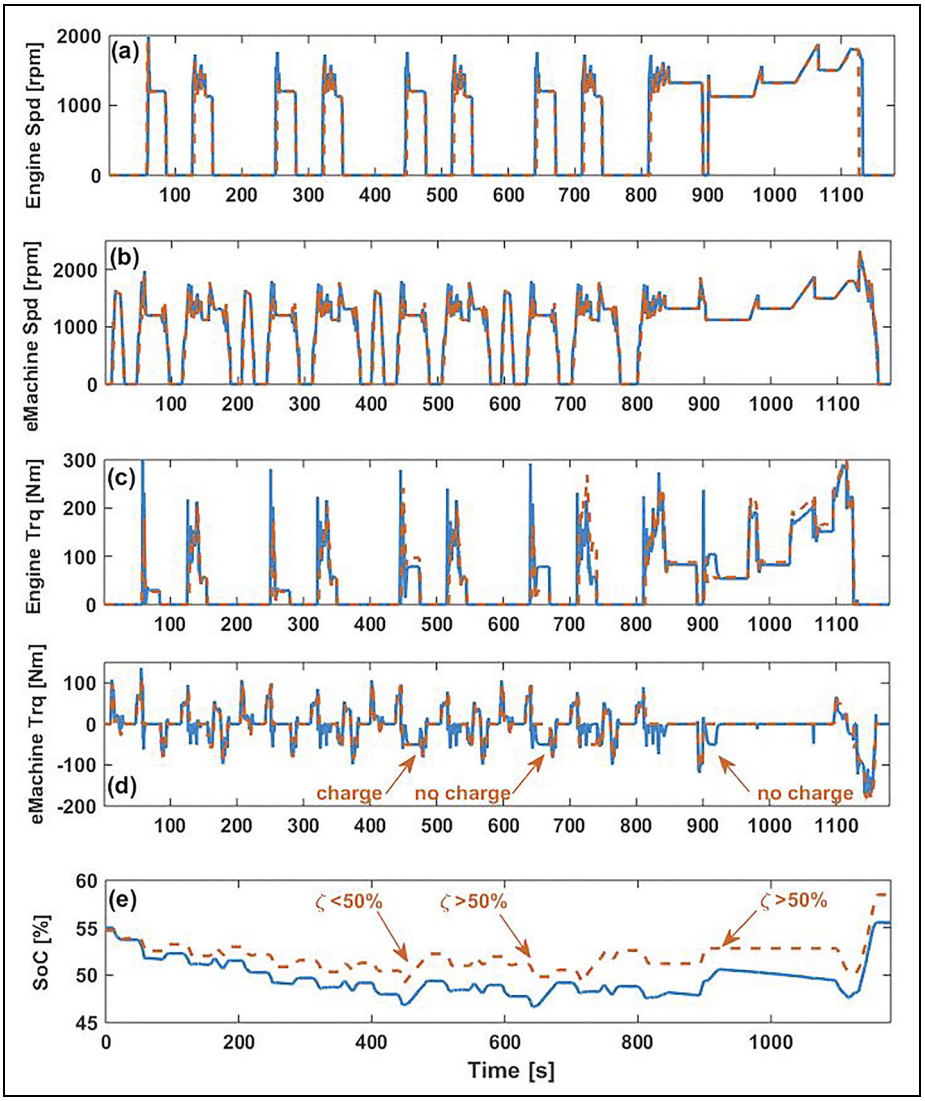

Figure 14. Verification of powertrain model (a) the engine speed and (b) the electric machine speed (c) engine torque, (d) electric machine torque (e) SoC solid curves, test results; dashed curves, simulation results.
eMachine: electric machine; Trq: torque; Spd: speed, SoC: state of charge.

hand, the thermal model is better simulated with the variable-step solvers of Dymola which are optimised to handle the non-linear behaviour of the refrigerant and air.[59] To achieve this, the thermal model was imported to Simulink using the FMI standard which enables Dymola solvers to be embedded in the exported code and to be used to simulate the code within Simulink.[60,61] Figure 15 shows the layout of the model and highlights the variability in local solvers. As the figure suggests, the thermal model uses two outputs of the powertrain model: first, the vehicle speed which is used to calculate the air flow through the condenser; second, the heat generation within the battery. In turn, the powertrain model receives the battery temperature and compressor power signals from the thermal model.

The controller block in Figure 15 includes the control algorithms of both the powertrain model and the thermal model; the former is described in WARPSTAR documents but the latter can be briefly explained as follows. The general requirement for cooling the battery is to keep its temperature between 30 °C and 35 °C. The cabin temperature should be maintained between 22 °C and 23 °C. A state machine is employed that uses the temperature limits to determine the operating state, i.e. the on–off switch of the compressor and the open–close flag of the refrigerant shut-off valves. The velocity of the compressor is controlled via two PI controllers, as seen in Figure 16(a). When the cabin is cooled, the compressor is controlled to maintain the evaporator temperature above 5 °C. When only battery cooling is active, the controller maintains the chiller temperature above 10 °C. Also, as shown in Figure 16(b), a third PI controller regulates the air flow from the blower on the basis of the cabin temperature.

Using the model, the vehicle energy consumption is calculated for hot ambient conditions (T_{air} = 35 °C; solar irradiance, 800 W/m^2) over the New European Driving Cycle (NEDC) and the Worldwide

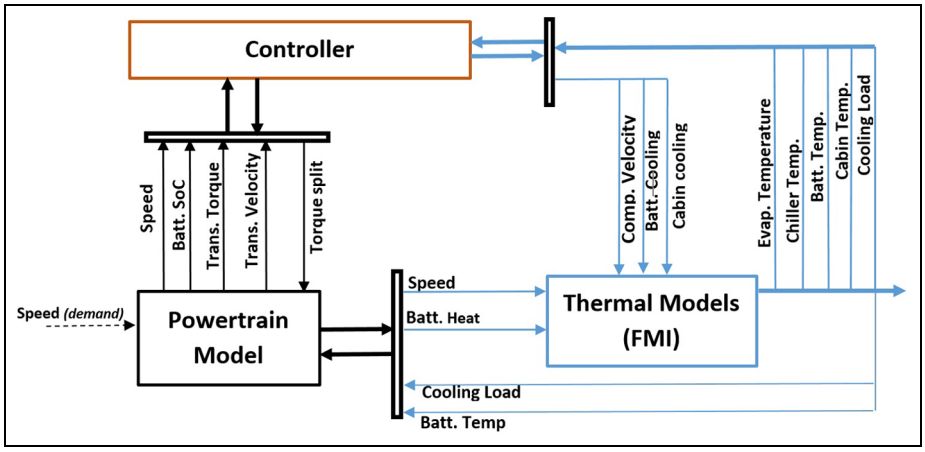

Figure 15. Layout of the system model in Simulink: the black border lines and arrows indicate the submodels and signals simulated using fixed-step MATLAB solvers; the blue border lines and arrows indicate the submodels and signals simulated with variable-step Dymola; the light brown rectangle indicates the controller.
Batt.: battery; SoC: state of charge; Trans.: transmission; Comp.: compressor; Temp.: temperature; Evap.: evaporator; FMI: Functional Mock-up Interface.

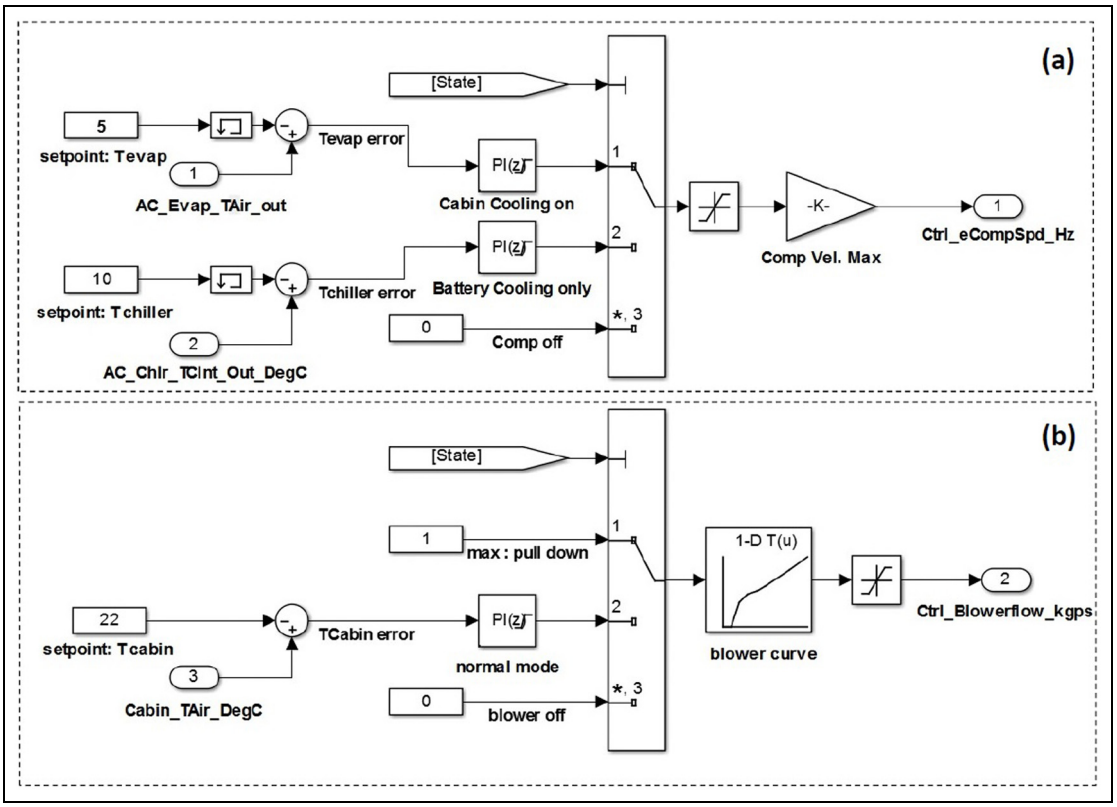

Figure 16. Control algorithm of the thermal model: (a) the compressor controller; (b) the blower controller.

Harmonised Light Vehicles Test Procedure (WLTP) cycle and the results are plotted in Figure 17. Figure 17(a) also shows the energy consumption for the standard 25 °C ambient condition (air conditioning off) as the baseline for comparisons. The baseline simulation results over the NEDC show an underestimation of 11% in the fuel consumption compared with the values reported for the vehicle, whereas the error is reduced to 4% for hot ambient conditions. This higher accuracy is expected because of the assumptions made in modelling the engine, since the temperature of the vehicle is closer to that assumed in the model. Figure 17(a) indicates that the cooling loads reduced the fuel economy of the vehicle by about 20%. It can be seen from Figure 17(b) that the model predicts that the cooling loads change the fuel economy over the WLTP cycle from 6.75 l/100

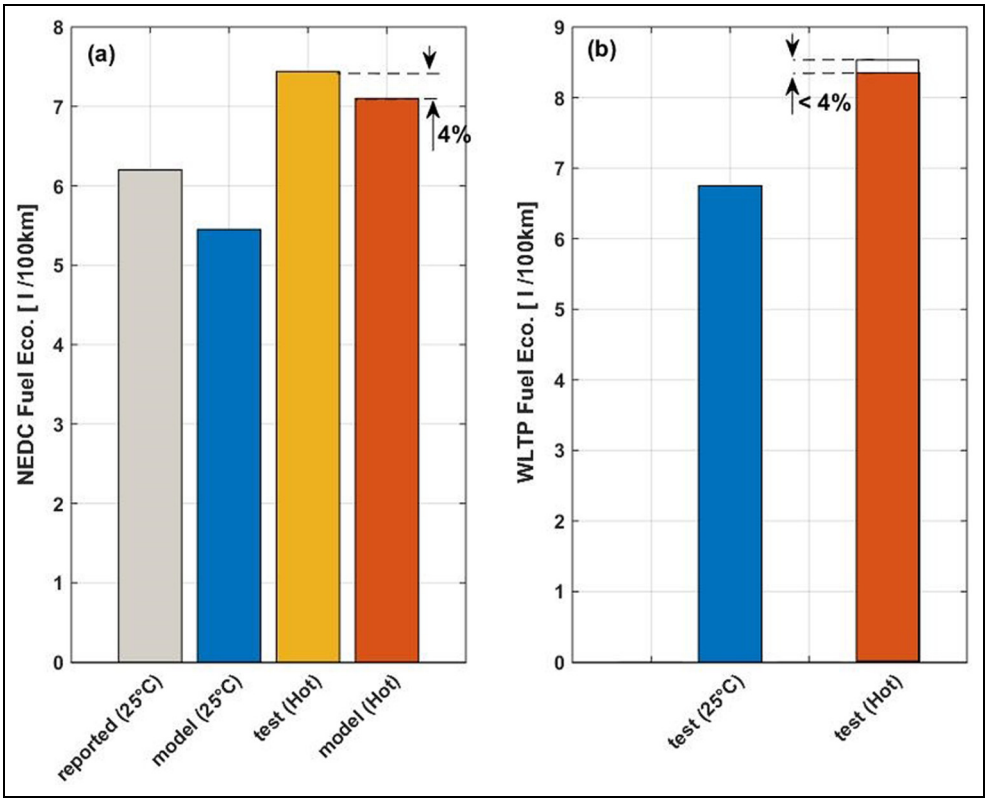

Figure 17. Vehicle-level energy consumption: (a) the converted energy; (b) the fuel economy.
NEDC: New European Driving Cycle; Eco.: economy; WLTP: Worldwide Harmonized Light Vehicles Test Procedure.

km to 8.35 l/100 km. It should be noted that, although reported figures or quotable test data are not available for the WLTP cycle, these results are consistent with the trends reported by Favre et al.[62] and that, since the WLTP cycle is significantly longer than the NEDC, using hot efficiency maps is more realistic; thus, an error of 4% or even less is expected.

As stated earlier, as well as accuracy, a suitable tool for vehicle-level calculations should have flexibility and a high speed. In terms of flexibility, the model can simulate various ranges of vehicle speed and ambient conditions. The only limitation is the zero flows of refrigerant and air which lead to discontinuities and cannot be handled by the air-conditioning submodel. Therefore, the compressor and blower controllers should include small offsets for which energy flows should be corrected accordingly. As for the simulation speed, some typical simulation times are given in Table 5. These results are achieved on a machine with a Core i7-2600 central processing unit and a 16 GB memory. Table 5 shows that the complete model is significantly slower than the powertrain model alone. Also, simulations with hotter ambient conditions are more time consuming since more events are generated in the model, e.g. because of more frequent opening and closing of the shut-off valves. Nevertheless, these simulation times are acceptable as they are considerably shorter than those reported for similar models by Kiss et al.[27] and Rasmussen.[63]

Table 5 Comparison of the simulation times.

Model	Simulation scenario	Duration (s)
Powertrain only	NEDC	19
	WLTP	26
Full model	NEDC (mild ambient)	286
	NEDC (hot ambient)	314
	WLTP (mild ambient)	346
	WLTP (hot ambient)	431

NEDC: New European Driving Cycle: WLTP: Worldwide Harmonized Light Vehicles Test Procedure.

Summary and conclusions

In this paper, a vehicle model was developed to enable the air-conditioning and battery-cooling loads to be included in vehicle-level energy efficiency calculations. Subsystem models were developed on the basis of the specifications of a target vehicle and integrated into Simulink using the FMI co-simulation standard. To achieve a representative model, verification against the experimental data from the target vehicle was embedded in the modelling process. The vehicle model developed here fulfils the requirements of the intended application as it is reasonably flexible, produces sufficiently accurate results and has an acceptable speed. One drawback of the modelling approach is its dependence on the test data. This dependence can be reduced

by using a more physics-oriented approach, e.g.in the case of the cabin. Additionally, this work highlighted the following.

1. When the aim is to obtain the overall conditions of the passenger cabin, a reduced-order model is adequate, and model calibrations such as those proposed here can help to avoid the burden of modelling the geometric details of the cabin.
2. Calibration of the heat transfer models in the battery-cooling plate and the heat exchangers were crucial in minimising the modelling and the computation effort.
3. A sufficiently accurate representation of the dynamics of the refrigeration circuit and the air-conditioning subsystem can be expected from a one-dimensional model such as those in the AirConditioning Library of Dymola despite various inherent simplifications. Dymola proved to be a flexible platform for implementing empirical correlations which played key roles in achieving a sufficiently accurate representation of the thermal processes with a low-order model.
4. This work reaffirmed that a purpose-built model can help to overcome the challenges of system-level simulations, i.e. balancing the accuracy and the speed. Here, subsystem-level verifications helped to determine the fidelity necessary for each submodel early in the modelling process, and awareness of the intended application allowed various simplifications. An example of such simplifications were the temperature-dependent variations in the efficiency of the powertrain which proved to be negligible for the intended application.

The model developed here is appropriate for analysing the energy requirement of air conditioning and battery cooling for hot ambient conditions and representative duty cycles similar those discussed by Shojaei et al.[64] These analyses can support the design of alternative thermal management strategies to reduce the impact of the cooling loads on the energy efficiency and performance of the vehicle. Although the correlations achieved above between the simulations and the test results are considered sufficient for this purpose, further development of some aspects of the model can enhance confidence in the subsequent analysis. Modelling the effect of the oil circulation in the refrigeration circuit and investigating its impact on the response of the model should be included in this development process. Also, additional investigations of the inaccuracies observed in the battery current signal that was logged from the controller area network of the vehicle is required to establish a possible requirement for higher fidelity to obtain the underlying reason.

Declaration of conflict of interest

The authors declare that there is no conflict of interest.

Funding

This work was supported by Innovative UK through the Warwick Manufacturing Group Centre High Value Manufacturing Catapult in collaboration with Jaguar Land Rover (EPSRC - EP/I01585X/1).

References

1. Rousseau A, Sharer P, Besnier F. Feasibility of Reusable Vehicle Modeling: Application to Hybrid Vehicles. In: *SAE Technical Paper*. 2004
2. Halbach S, Sharer P, Pagerit S et al. Model architecture, methods, and interfaces for efficient math-based design and simulation of automotive control systems. SAE paper 2010-01-0241, 2010.
3. Markel T, Brooker A, Hendricks T et al. ADVISOR: a systems analysis tool for advanced vehicle modeling. *J Power Sources* 2002; 110: 255–266.
4. Walker A, McGordon A, Hannis G et al. A novel structure for comprehensive HEV powertrain modelling. In: *2006 IEEE vehicle power and propulsion conference*, Windsor, Berkshire, UK, 6–8 September 2006, pp. 1–5. New York: IEEE.
5. Gopal RV and Rousseau AP. System analysis using multiple expert tools. SAE paper 2011-01-0754, 2011.
6. Abel A, Blochwitz T and Eichberger A. Functional mock-up interface in mechatronic gearshift simulation for commercial vehicles. In: *9th international Modelica conference*, Munich, Germany, 3–5 September 2012, pp. 775–780. Linköping: Modelica Association.
7. Macbain JA, Conover JJ and Brooker AD. Full vehicle simulation for series hybrid vehicles. SAE paper 2003-01-2301, 2003.
8. Johnson V. Battery performance models in ADVISOR. *J Power Sources* 2002; 110: 321–329.
9. Samhaber C, Wimmer A and Loibner E. Modeling of engine warm-up with integration of vehicle and engine cycle simulation. SAE paper 2001-01-1697, 2001.
10. Puntigam W, Balic J, Almbauer R et al. Transient co-simulation of comprehensive vehicle models by time dependent coupling. SAE paper 2006-01-1604, 2006.
11. Dvorak D, Thomas B, Rathberger C et al. Thermal vehicle-concept study using co-simulation for optimizing driving range. In: *2015 IEEE vehicle power and propulsion conference*, Montreal, Quebec, Canada, 19–22 October 2015, pp. 1–6. New York: IEEE.
12. Regner G, Loibner E and Krammer J. Analysis of transient drive cycles using CRUISE-BOOST co-simulation techniques. SAE paper 2002-01-0627, 2002.
13. Samadani E, Fraser R and Fowler M. Evaluation of air conditioning impact on the electric vehicle range and Li-ion battery life. SAE paper 2014-01-1853, 2014.
14. Gao GG. Investigation of climate control power consumption in DTE estimation for electric vehicles power usage of climate control. SAE paper 2014-01-0713, 2014.
15. Kambly KR and Bradley TH. Estimating the HVAC energy consumption of plug-in electric vehicles. *J Power Sources* 2014; 259: 117–124.

16. Rugh J and Farrington R. Vehicle ancillary load reduction project close-out report. Technical Report NREL/TP-540-42454, National Renewable Energy Laboratory, Golden, Colorado, USA, 2008.
17. Farrington RB, Anderson R, Blake DM et al. Challenges and potential solutions for reducing climate control loads in conventional and hybrid electric vehicles. Report, National Renewable Energy Laboratory, Golden, Colorado, USA, 1999.
18. Rugh JA, Pesaran A and Smith K. Electric vehicle battery thermal issues and thermal management techniques. In: *SAE alternative refrigerant and system efficiency symposium*, Scottsdale, Arizona, USA, 27–29 September 2012, pp. 1–40. Warrendale, Pennsylvania: SAE International.
19. Krüger IL, Limperich D and Schmitz G. Energy consumption of battery cooling in hybrid electric vehicles. In: *14th international refrigeration and air conditioning conference*, West Lafayette, Indiana, USA, 16–19 July 2012, paper 2334, pp. 1–10. West Lafayette, Indiana: Purdue University Press.
20. Neubauer J and Wood E. Thru-life impacts of driver aggression, climate, cabin thermal management, and battery thermal management on battery electric vehicle utility. *J Power Sources* 2014; 259: 262–275.
21. Roscher MA, Leidholdt W and Trepte J. High efficiency energy management in BEV applications. *Int J Electr Power Energy Systems* 2012; 37: 126–130.
22. Shojaei S, Robinson S, Chatham C et al. Modelling the electric air conditioning system in a commercially available vehicle for energy management optimisation. SAE paper 2015-01-0331, 2015..
23. Khayyam H and Bab-Hadiashar A. Adaptive intelligent energy management system of plug-in hybrid electric vehicle. *Energy* 2014; 69: 319–335.
24. Huang D, Öker E, Yang S-L et al. A dynamic computer-aided engineering model for automobile climate control system simulation and application Part I: A/C component simulations and integration. SAE paper 1999-01-1195, 1999.
25. Joudi KA, Mohammed ASK and Aljanabi MK. Experimental and computer performance study of an automotive air conditioning system with alternative refrigerants. *Energy Conversion Managmt* 2003; 44: 2959–2976.
26. Zhang Q and Canova M. Lumped-parameter modeling of an automotive air conditioning system for energy optimization and management. In: *ASME 2013 dynamic systems and control conference, Vol 1: aerial vehicles; aerospace control; alternative energy; automotive control systems; battery systems; beams and flexible structures; biologically-inspired control and its applications; biomedical and bio-mechanical systems; biomedical robots and rehab; bipeds and locomotion; control design methods for advanced powertrain systems and components; control of adv. combustion engines, building energy systems, mechanical systems; control, monitoring, and energy harvesting of vibratory systems*, Palo Alto, California, USA, 21–23 October 2013, paper DSCC2013-3835, pp. V001T04A003-1–V001T04A003-8. New York: ASME.
27. Kiss T and Lustbader J. Comparison of the accuracy and speed of transient mobile A/C system simulation models. SAE paper 2014-01-0669, 2014.
28. Ling J, Eisele M, Qiao H et al. Transient modeling and validation of an automotive secondary loop air-conditioning system. SAE paper 2014-01-0647, 2014.
29. Modelon. Air Conditioning Library, http://www.modelon.-com/products/modelica-libraries/air-conditioning-library/ (2015, accessed 10 December 2016).
30. Tummescheit H, Eborn J and Prölss K. Airconditioning – a Modelica library for dynamic simulation of AC systems. In: *4th international Modelica conference*, Hamburg, Germany, 7–8 March 2005, pp. 185–192. Linköping: Modelica Association.
31. Tummescheit H, Eborn J and Wagner FJ. Development of a Modelica base library for modeling of thermo-hydraulic systems. In: *Modelica workshop*, Lund, Sweden, 23–24 October 2000, pp. 41–51. Linköping: Modelica Association.
32. Blochwitz T, Otter M and Åkesson J. Functional Mockup Interface 2.0: the standard for tool independent exchange of simulation models. In: *9th international Modelica conference*, Munich, Germany, 3–5 September 2012, pp. 173–184. Linköping: Modelica Association.
33. Nielsen F, Gullman S, Wallin F et al. Simulation of energy used for vehicle interior climate. SAE paper 2015-01-9116, 2015.
34. Khamsi Y and Petitjean C. Validation results of automotive passenger compartment and its air conditioning system modeling. *Fuel* 2000; 2013: 7–9.
35. Jha KK, Bhanot V and Ryali V. A simple model for calculating vehicle thermal loads. SAE paper 2013-01-0855, 2013.
36. Zhang H, Dai L, Xu G et al. Studies of air-flow and temperature fields inside a passenger compartment for improving thermal comfort and saving energy. Part I: test/numerical model and validation. *Appl Thermal Engng* 2009; 29: 2022–2027.
37. Nagano H, Miyamoto I and Kohri I. Numerical analysis of energy efficiency of zone control air-conditioning system for electric vehicle using numerical manikin. SAE paper 2013-01-0237, 2013.
38. Ingersoll JG, Kalman TG, Maxwell LM et al. Automobile passenger compartment thermal comfort model – Part I: compartment cool-down/warmup calculations. SAE paper 920266, 1992.
39. Fujita A, Kanemaru J, Nakagawa H et al. Numerical simulation method to predict the thermal environment inside a car cabin. *JSAE Rev* 2001; 22: 39–47.
40. Ling J, Aute V, Hwang Y et al. A new computational tool for automotive cabin air temperature simulation. SAE paper 2013-01-0868, 2013.
41. Kaynakli O, Pulat E and Kilic M. Thermal comfort during heating and cooling periods in an automobile. *Heat Mass Transfer* 2005; 41: 449–458.
42. Zheng Y, Mark B and Youmans H. A simple method to calculate vehicle heat load. SAE paper 2011-01-0127, 2011.
43. Huang D, Öker E, Yang S-L et al. A dynamic computer-aided engineering model for automobile climate control system simulation and application Part II: passenger compartment simulation and applications. SAE paper 1999-01-1196, 1999.
44. Kiss T, Chaney L and Meyer J. A new automotive air conditioning system simulation tool developed in MATLAB/Simulink. SAE paper 2013-01-0850, 2013.
45. Rijnders A. Mobile airconditioning test procedure. Informal Document GRPE-64-23, United Nations Economic Commission for Europe, Geneva, Switzerland, 2012.

46. Pesaran AA. Battery thermal models for hybrid vehicle simulations. *J Power Sources* 2002; 110: 377–382.
47. Karnik AY, Fuxman A, Bonkoski P et al. Vehicle powertrain thermal management system using model predictive control. SAE paper 2016-01-0215, 2016.
48. Casella F, Otter M, Proelss K et al. The Modelica Fluid and Media Library for modeling of incompressible and compressible thermo-fluid pipe networks. In: *5th international Modelica conference*, Vienna, Austria, 4–5 September 2006, pp. 631–640. Linköping: Modelica Association.
49. MAGNA. Kuli software, http://www.kuli-software.com/KULI.497.0.html (2016, accessed 29 February 2016).
50. National Renewable Energy Laboratory. CoolSim, http://www.nrel.gov/vehiclesandfuels/vtm_models_tools.html.
51. Braun M, Caesar R, Limperich D et al. Simulation of a vehicle refrigeration cycle with Dymola/Modelica. SAE paper 2005-01-1899, 2005.
52. Eborn J. *On model libraries for thermo-hydraulic applications*. Lund Institute of Technology, 2001
53. Tummescheit H. *Design and Implementation of Object-Oriented Model Libraries using Modelica*. Lund Institute of Technology, 2002
54. Incropera FP. *Fundamentals of heat and mass transfer*. New York: John Wiley, 2011.
55. Gnieleinski V. Heat transfer in pipe flows. In: *VDI heat atlas*. Berlin: Springer, 2010, ch G1, pp. 693–700.
56. Rasmussen BP and Alleyne AG. Control-oriented modeling of transcritical vapor compression systems. *Trabs ASME, J Dynamic Systems Measmt Control* 2004; 126: 54–64.
57. Orofino L, Amante F, Mola S et al. An Integrated approach for air conditioning and electrical system impact on vehicle fuel consumption and performances analysis: DrivEM 1.0. SAE paper 2007-01-0762, 2007.
58. European Commission. Commission Regulation (EC) No 692/2008 of 18 July 2008 implementing and amending Regulation (EC) No 715/2007 of the European Parliament and of the Council on type-approval of motor vehicles with respect to emissions from light passenger and commercial vehicles (Euro 5 and Euro 6) and on access to vehicle repair and maintenance information. *Off J Eur Union* 2008; L 199: 1–136.
59. Liu L, Felgner F and Frey G. Comparison of 4 numerical solvers for stiff and hybrid systems simulation. In: *15th 2010 IEEE international conference on emerging technologies and factory automation*, Bilbao, Spain, 2010, pp. 1–8. New York: IEEE.
60. *Functional mock-up interface, FMI support in Dymola*. Vélizy-Villacoublay: Dassault Systèmes AB.
61. Lawrence Livermore National Laboratory. SUNDIALS: SUite of Nonlinear and DIfferential/ALgebraic Equation Solvers https://computation.llnl.gov/projects/sundials (accessed 1 December 2016).
62. Favre C, Bosteels D and May J. Exhaust emissions from European market – available passenger cars evaluated on various drive cycles. SAE paper 2013-24-0154, 2013.
63. Rasmussen BP. Dynamic modeling for vapor compression systems – Part I: literature review. *HVAC&R Res* 2012; 18: 934–955.
64. Shojaei S, Robinson S, McGordon A et al. Passengers vs. battery: calculation of cooling requirements in a PHEV. SAE paper 2016-01-0241, 2016.

Appendix I

Notation

A_{aw}	air-side heat transfer area of the heat exchanger (air-conditioning subsystem) (m^2)
A_g	area of glass in the cabin shell (cabin subsystem) (m^2)
A_{wr}	refrigerant-side heat transfer area of the heat exchanger (air-conditioning subsystem) (m^2)
c_{clnt}	specific heat capacity of the coolant (battery-cooling subsystem) (kJ/kg K)
C_{batt}	specific heat capacity of the battery (battery-cooling subsystem) (kJ/K)
$\bar{h}_{aw}$	average air-side heat transfer coefficient of the heat exchanger (air-conditioning subsystem) (W/m^2 K)
$\bar{h}_{wr}$	average refrigerant-side heat transfer coefficient of the heat exchanger (air-conditioning subsystem) (W/m^2 K)
I_{eq}	equivalent inertia of the vehicle (powertrain subsystem) (kg m^2)
$\dot{m}_{clnt}$	mass flow rate of the coolant (battery-cooling subsystem) (kg/s)
M	mass of the vehicle (powertrain subsystem) (kg)
Nu	Nusselt number
Pr	Prandtl number (air-conditioning subsystem)
$\dot{Q}_{amb}$	heat flow between the battery and the ambient (battery-cooling subsystem) (W)
$\dot{Q}_{cabin}$	heat flow between the cabin and the ambient (battery-cooling subsystem) (W)
$\dot{Q}_{clnt}$	heat flow between the battery and the ambient (battery-cooling subsystem) (W)
$\dot{Q}_{gen}$	internal heat generation of the battery (battery-cooling subsystem) (W)
$\dot{Q}^{irr}_{g,\,abs}$	solar irradiance absorbed by the glass (cabin subsystem) (W)
$\dot{Q}^{irr}_{g,\,tr}$	solar irradiance transmitted through the glass (cabin subsystem) (W)
$\dot{Q}^{irr}_{int,\,abs}$	solar irradiance absorbed by the interior (cabin subsystem) (W)
R_{amb}	battery–ambient heat transfer resistance (battery-cooling subsystem) (K/W)
R_{cabin}	battery–cabin heat transfer resistance (battery-cooling subsystem) (K/W)
$\bar{R}_{clnt}$	battery–coolant heat transfer resistance (battery-cooling subsystem) (K/W)
Re	Reynolds number (air-conditioning subsystem)
T_{air}	temperature of the air stream (air-conditioning subsystem) (K)
T_{amb}	ambient temperature (battery-cooling subsystem) (K)
T_{batt}	lumped battery temperature (battery-cooling subsystem) (K)

$T_{cabin,int}$ temperature of the cabin interior (cabin subsystem) (K)
$T_{clnt,in}$ temperature of the coolant at the battery inlet (battery-cooling subsystem) (K)
$T_{clnt,out}$ temperature of the coolant at the battery outlet (battery-cooling subsystem) (K)
T_r temperature of the refrigerant in the heat exchanger (air-conditioning subsystem)
T_w temperature of the heat exchanger wall (air-conditioning subsystem)
α_g average absorptivity of the glass (cabin subsystem)
θ throttle opening (powertrain subsystem) (%)
τ_{em} torque of the electric machine (powertrain subsystem) (N m)
τ_{eng} torque of the engine (powertrain subsystem) (N m)
τ_g average transmissivity of the glass (cabin subsystem)

Abbreviations

EV electric vehicle
HEV hybrid electric vehicle
FMI Functional Mock-up Interface
IHX internal refrigerant–refrigerant heat exchanger
NEDC New European Driving Cycle
PI proportional–integral
SI solar irradiance (cabin subsystem) (W/m^2)
SoC state of charge
TXV thermostatic expansion valve
WLTP Worldwide Harmonized Light Vehicles Test Procedure